Journal of Oceanography
Vol. 52, pp. 771 to 784. 1996

Wind-Induced Kuroshio Intrusion into the South China Sea

AMY FARRIS and MARK WIMBUSH

University of Rhode Island, Narragansett, RI 02882-1197, U.S.A.

(Received 10 February 1996; in revised form 9 May 1996; accepted 12 May 1996)

The Kuroshio flows north along the east coasts of the Philippines and Taiwan. Between these two land masses lies the Luzon Strait which connects the Pacific Ocean to the South China Sea. The Kuroshio usually flows north past this strait, but at times part or all of it flows west through the strait into the South China Sea forming a loop current. It has been suggested that the loop current forms when the northeast monsoon deflects the Kuroshio through the Luzon Strait. In this study, satellite-derived sea-surface temperature images are used to observe the Kuroshio in the Luzon Strait region. Together with wind data from the region, these observations indicate a loop-current development process which is largely determined by an integrated supercritical wind stress parameter. The loop current grows when a four-day average of the local wind-stress component directed to the south exceeds 0.08 Nm^{-2}. When this average wind-stress component drops below the critical value, the Kuroshio returns to its northward path.

1. Introduction

The Kuroshio is the principal western boundary current of the North Pacific. It is formed from the branching of the North Equatorial Current off the east coast of the Philippines, usually between 11°N and 14.5°N (Nitani, 1972). The southward flowing branch is called the Mindanao Current, and the northward flowing branch is called the Kuroshio. The Kuroshio flows north along the east coast of the Philippines until it passes the island of Luzon where it encounters the Luzon Strait. The strait is about 350 km wide and is 2500 m deep at its deepest point. The Kuroshio usually continues north past this strait to flow along the east coast of Taiwan (Fig. 1(a)). Occasionally, however, part or all of the Kuroshio penetrates through the Luzon Strait into the northern South China Sea, forming a loop current (Su *et al.*, 1990) (Fig. 1(b)). When this happens, part or all of the Kuroshio flows to the west through the Luzon Strait just north of 20°N. The water may travel as far west as about 117°E before turning north and then east, apparently following the shelf break southwest of Taiwan (Huang, 1988; Wang and Chern, 1988). Part of this water may enter the Taiwan Strait; it is generally thought that some Kuroshio water occasionally flows north through the eastern side of the Taiwan Strait (Fan, 1982; Wang and Chern, 1987a) (Fig. 1(b)). The Kuroshio east of Luzon and Taiwan is on average 140 km wide (Su *et al.*, 1990) and is roughly 800 m deep (Nitani, 1972). Its maximum velocity is 1–1.5 ms^{-1} (Su *et al.*, 1990), while the volume transport is between 28 and 43 Sv (Nitani, 1972; Guo and Wendong, 1988).

It is not known when or how often the loop current is present. Chu (1972) suggests part of the Kuroshio always flows west through the Luzon Strait; but absence of the loop current has been reported several times (Nitani, 1972; Uda and Nakao, 1973; Huang, 1988). Wang and Chern (1987b) propose that the loop current forms only during the northeast monsoon season. The winds in this region are monsoonal, typically blowing strongly from the northeast during September through March and weakly from the southwest during April through August. We

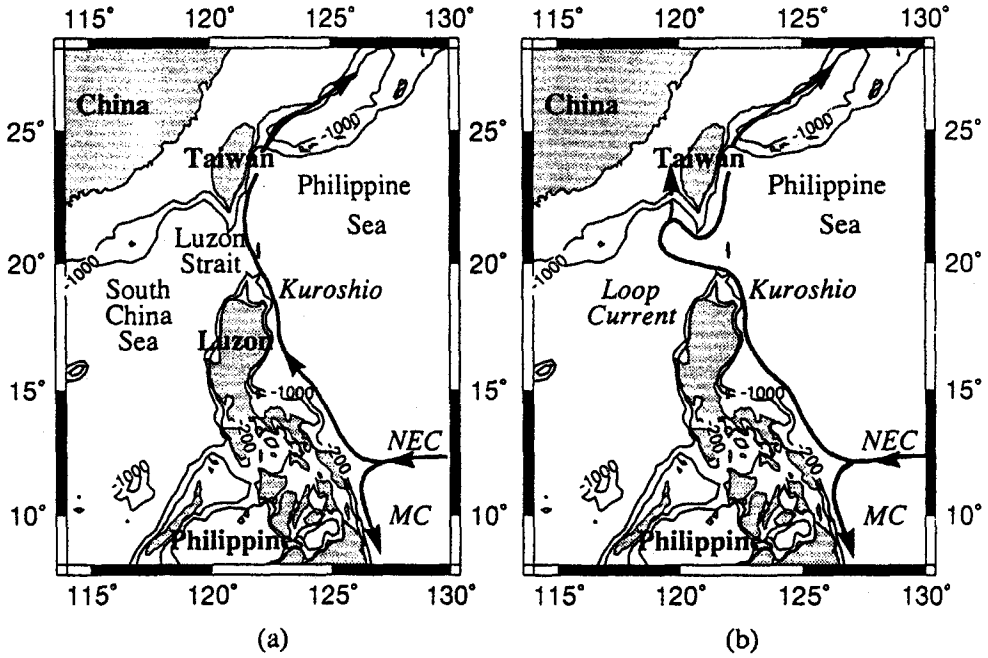

Fig. 1. The region in which the Kuroshio originates. MC = Mindanao Current, NEC = North Equatorial Current. Depth contours shown are for 200 m and 1000 m. (a) Direct Kuroshio path across Luzon Strait, (b) Kuroshio loop current through Luzon Strait into South China Sea.

found no reports of a loop current during the southwest monsoon season; but there are reports of a westward flow in the Luzon Strait during September (Chu, 1972; Nitani, 1972; Guo and Wendong, 1988), which is the transitional month between the southwest and northeast monsoons.

It is not known what causes the formation of the loop current or how it develops. Shaw (1991) suggests loop current formation may be related to changes in Kuroshio transport. According to the theory put forward by Wang and Chern (1987b), the northeast monsoon causes Ekman transport which deflects the Kuroshio westward through the Luzon Strait. Similarly in models of the Gulf Stream, Adamec and Elsberry (1985) and Xue *et al.* (1995) have shown that frontal position is strongly influenced by Ekman-like advection.

It is important to understand the loop current process because the South China Sea is one of the world's largest marginal seas and the Luzon Strait is its principal connection to the surrounding ocean. Intrusions of the Kuroshio through this strait affect the circulation and water chemistry of the South China Sea. The surface waters of the South China Sea are seasonally variable and relatively fresh, whereas the Kuroshio water is warm, salty and has little seasonal variation (Chu, 1972).

2. Background

In conducting a hydrographic survey during April of 1974, Wang and Chern (1987a) found evidence of an anti-cyclonic eddy in the northern South China Sea. They determined that the eddy had a diameter of 200 km, a depth of 100 m and was comprised of Kuroshio water. They hypothesized that this eddy was the result of Ekman transport of the Kuroshio by the northeast monsoon. In a second paper they proposed a theory for this mechanism (Wang and Chern,

1987b). They assumed a representative steady wind stress in the Luzon Strait from the northeast of 1.5 dynes cm^{-2} = 0.15 Nm^{-2} (speed = 10.5 ms^{-1}). From this wind stress and the width of the Luzon Strait, they calculated an Ekman transport of 4.6×10^5 m^3s^{-1}. In order to estimate how long it took for the eddy to form, they divided the volume of the eddy by this volume transport and obtained an estimate of 90 days.

The Kuroshio has flow depth greater than the 100 m eddy depth observed by Wang and Chern (1987b). It is unclear what happens to the deeper Kuroshio flow when the loop current forms.

3. Data

This work compares satellite observations of loop current development with ship measurements of the wind field, in order to investigate the hypothesis that the loop current is formed in response to the northeast monsoon. We first examined sea-surface temperature images to find and characterize loop-current events. We also examined Geosat altimetry data for evidence of loop-current occurrences, but had only modest success; the loop current was barely discernible from the background fluctuations in the Geosat data (Farris, 1995; Appendix A). We then analyzed wind data to look for possible relationships between these loop-current events and the wind field.

3.1 Sea-surface temperature data

The sea-surface temperature images used in this study are from the Jet Propulsion Laboratory Oceans Pathfinder data set (Vazquez *et al.*, 1995). Advanced Very High Resolution Radiometers on several NOAA/TIROS satellites collected images of the region twice a day, with 0.15°C resolution in temperature and 4 km resolution in space. After Pathfinder processing, the spatial resolution is 9 km. The images were declouded with the algorithm developed by Cayula (1993). We visually examined each sea-surface temperature image for 1987, 1988 and 1989 (the years for which Pathfinder data were available) looking for clear images of the Kuroshio in the Luzon Strait region.

During winter and spring it is very easy to see Kuroshio surface waters in this region because they are much warmer than the surrounding surface waters in the Luzon Strait and South China Sea. During the summer months however, the South China Sea water warms significantly. This causes a decrease in the temperature difference between the Kuroshio and South China Sea surface waters, making it difficult to distinguish the two water masses. There is usually a month or two (August, September) when it is impossible to distinguish the two water masses and tell if a loop current is present.

One problem with satellite thermal images is that clouds block the infra-red radiation preventing measurements in cloudy areas. Since it is often cloudy in this region, there are many gaps in the sea-surface temperature record. During the northeast monsoon, anywhere from 56% to 90% of the images are mostly or completely cloudy. Additionally, thin clouds may block only part of the radiation coming from the water and make the water appear cooler than it actually is. With practice, most of these instances can be recognized, but one should always be aware of the problem.

There is another reason one should be careful in interpreting sea-surface temperature images. Because the satellite measures only the top millimeter of the ocean, diurnal warming is a common problem. During a sunny day with light winds, a very thin surface layer may warm significantly (Stramma *et al.*, 1986). Thus day images may be warmer than night images. Whenever possible, we used only night images.

3.2 *Wind data*

The wind data used in this study are from the ship-reported data in the Comprehensive Ocean Data Set from the National Center for Atmospheric Research. Reported winds at various elevations were all scaled to 10 meters above the surface, using the method of Da Silva mentioned in Fanning *et al.* (1994). When quality control flags indicated suspect data, those data were ignored. Wind stress $\vec{\tau}$ in Nm^{-2} was estimated from wind velocity $\vec{U}_{10}$ at 10 m, through the relation $\vec{\tau} = \rho_a C_{10} U_{10} \vec{U}_{10}$, where $\rho_a = 1.3$ kg m^{-3} is the density of air, drag coefficient $C_{10} = (0.8 + 0.065 U_{10}) \times 10^{-3}$, and $U_{10} (= |\vec{U}_{10}|)$ is the wind speed in ms^{-1} (Wu, 1982). We then vectorially averaged this stress over a 4° × 4° box centered at 20°N, 120°E and over one-day intervals. The average number of data points contributing to each one-day average was 15, the maximum and minimum were 60 and 1 respectively. If this number fell below four, the average values were examined to confirm that they were reasonable (compared with the previous and following days' averages). Figure 2 is a plot of this daily averaged wind stress, showing both magnitude and direction. The northeast monsoon can be seen as strong winds blowing toward 225°, typically beginning in September and continuing through March.

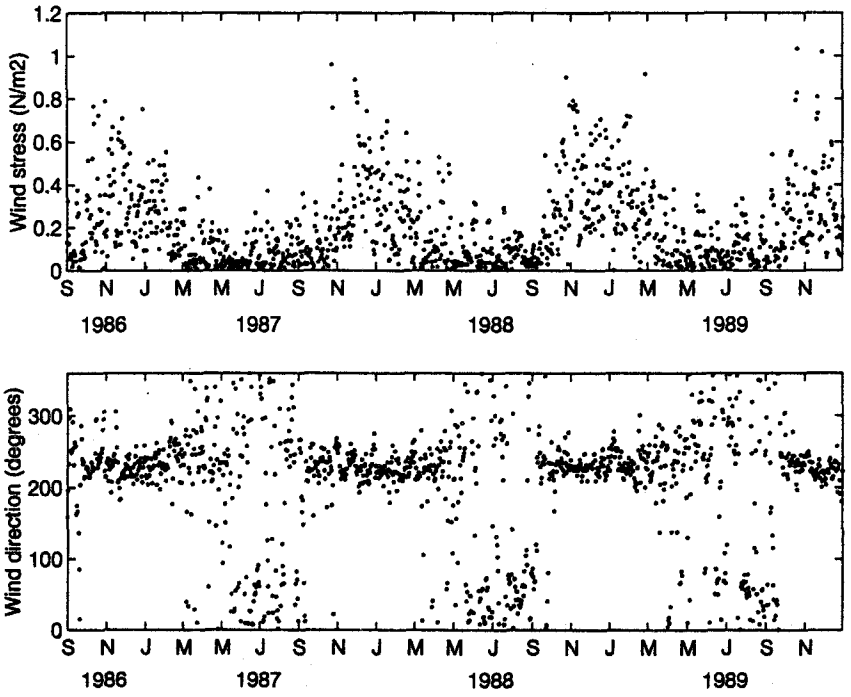

Fig. 2. Daily vector-averaged wind stress in the Luzon Strait region from September 1986 through December 1989. Time axis tick marks are at 2-month intervals. They correspond to the first day of a month and are labeled with that month's initial letter. Upper panel is stress magnitude (Nm^{-2}). Lower panel is compass direction in degrees (true) toward which the stress is directed. The northeast monsoon can be seen as stronger winds coming consistently from the northeast (i.e., towards about 225°) beginning about September and lasting through about March. During the southwest monsoon, the winds are not as strong nor is the direction as steady.

4. Results

4.1 Describing loop-current development

Although the entire development sequence of one loop current was never observed, different stages were seen in different years so that we can hypothesize the four-stage development sequence shown in Fig. 3. Stage 0 represents the "normal" path of the Kuroshio. Figure 4 is a sea-surface temperature image of typical Stage 0 conditions. The loop current begins in Stage 1 with the Kuroshio moving slightly westward, so instead of being directed to the east of Taiwan, it flows towards the southern tip of Taiwan. There are several images that show the Kuroshio

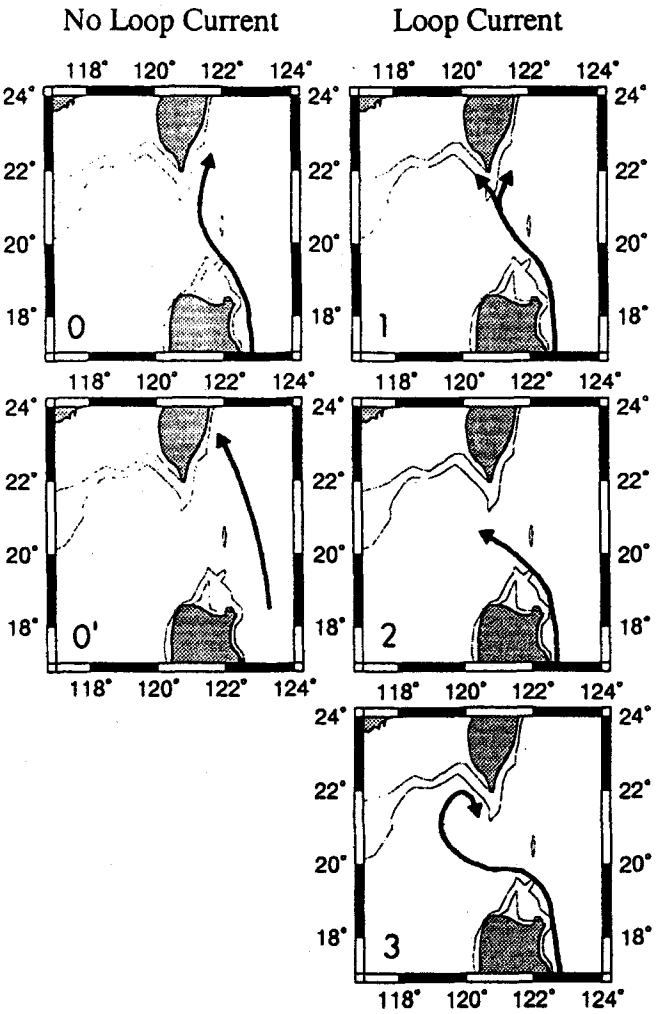

Fig. 3. Representative sketches of the Kuroshio loop current in the Luzon Strait in different stages of development, from Stage 0 (no deflection) to Stage 3 (fully-developed loop current). A prime, as in Stage 0′, indicates a Kuroshio displaced to the east. Dotted lines are the 200 m and 1000 m isobaths. The Kuroshio path is shown as a broad line.

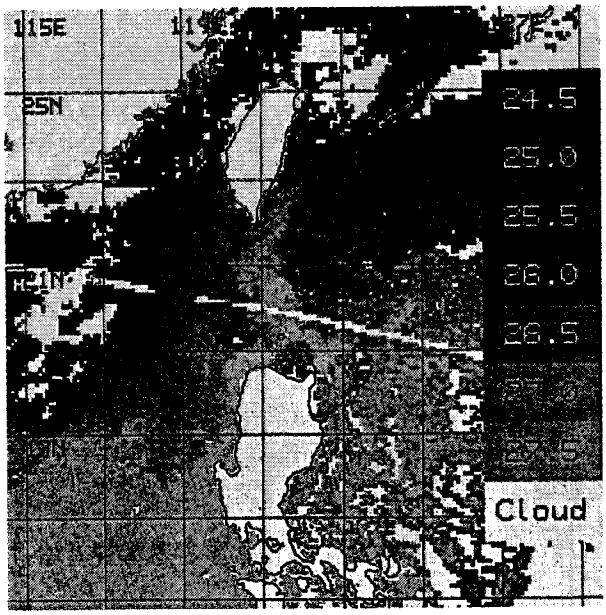

Fig. 4. Sea-surface temperature image from March 14, 1988; loop current in Stage 0.

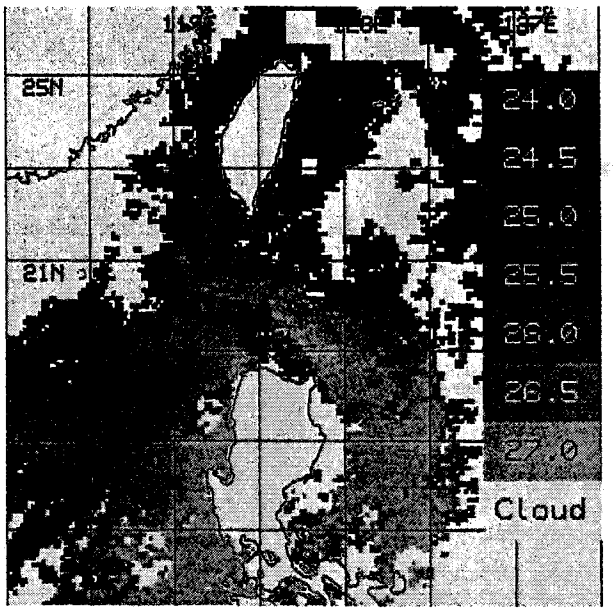

Fig. 5. Sea-surface temperature image from December 7, 1988, loop-current in Stage 3.

bifurcating at the southern tip of Taiwan. As the loop current develops further, the Kuroshio pivots towards the west, with a pivot point at 20°N. South of 20°N there is a shelf (0–1000 m depth) in the Luzon Strait that seems to prevent penetration of the Kuroshio. In Stage 2 the Kuroshio is directed to the west of Taiwan. With further development, a full loop is eventually formed in Stage 3. Figure 5 is a sea-surface temperature image of a typical Stage 3 loop current. Also shown in Fig. 3 is Stage 0′. The prime indicates that the Kuroshio is further east than normal (around 122.5°E instead of 121°E at 21°N). The prime is added to any loop current stage where the main portion of the Kuroshio is significantly further east than normal.

In many of the images, both a loop-current path and a direct path appear for the Kuroshio. We designate all such images as 2–0 or 3–0 depending on whether the loop current is in Stage 2 or 3. From the thermal images we cannot determine the proportions of the Kuroshio flow that are carried in these two branches.

4.2 Finding loop-current occurrences

Having defined these stages of loop-current development, we went back through all the sea-surface temperature images and numbered each clear image according to the observed stage of the loop current. Unless an image was unusually clear, we made these determinations only when there were at least two images showing the same feature in a two-day interval. (We took this precaution because of the problems mentioned in Subsection 3.1.) In the three years of sea-surface temperature data (1987, 1988, 1989), there were 43 times that loop-current stage determinations could be confidently made. Multiple images taken within four days were counted as one observation if they all showed the same feature.

In the three years of sea-surface temperature data we made 13 observations of loop currents (i.e., stages other than 0 or 0′). All of these observations were during the months November through March. (There were a total of 23 observations during these months and 20 observations during the other months.) Since the northeast monsoon typically begins in September and lasts through March (Shaw and Chao, 1994), this suggested a relationship between the loop current and the northeast monsoon, but with a delay in loop-current formation. The form of this relationship will be investigated in the next section.

4.3 Comparison with wind

In our first attempt at seeking the form of the relationship between the wind and loop-current stage, we averaged the wind in various ways on the supposition that the loop current might respond to some weighted average of the past wind stress. We tried computing block, linearly-tapered and exponentially-tapered averages over times from two weeks to six months and tested the hypothesis that the loop current forms when a trailing average exceeds some critical value. No single choice of averaging shape, duration and critical stress level gave satisfactory agreement with the loop-current observations.

We then tested a prediction scheme based on the hypothesis that when the wind stress exceeds some critical level the loop current is formed by the time-integrated wind stress. On this hypothesis, Stage 0 conditions prevail when τ, the southward component of the wind stress, stays below a critical value τ_c. Resulting westward flow is then low enough that it is entrained into the Kuroshio from the east, and detrained to the west, without disturbing the Kuroshio position. When τ exceeds τ_c, the Kuroshio begins to be deflected at a rate which is proportional to the stress in excess of τ_c. (We assume the non-entrained flow is proportional to the excess stress.) The loop current then grows through the stages described in Subsection 4.1 until the wind stress drops

below τ_c. When this occurs, the Kuroshio reverts to its direct path across the Luzon Strait. Since total deflection is the integral of the rate, this idea can be expressed mathematically by defining an integrated supercritical wind stress parameter Ω as

$$\Omega(t) = \int_{t_c}^{t} \mathcal{R}_{1/2}(\tau - \tau_c)dt \tag{1}$$

where $\mathcal{R}_{1/2}(x) = \frac{1}{2}(x + |x|)$ is the half-wave rectifier function, t is the present time, and t_c is the nearest preceding time at which $\overline{\tau}$, an average over the previous $t_{ave} = 4$ days of this southward wind-stress component, was less than $\tau_c = 0.08$ Nm^{-2}.

Figure 6 shows $\Omega(t)$ computed in this way from our wind-stress time series for fall and winter of each year, from September of 1986 through December of 1989. Also shown are the times at which clear interpretations of loop-current state could be made from satellite data (vertical lines) together with the determined stage numbers according to our scheme shown in Fig. 3. Spring and summer seasons are not shown in this figure, because throughout those times (which are predominantly times of the southwest monsoon) $\Omega(t)$ is zero and there are no indications in the temperature data of any loop currents, during these years. (As explained in Subsection 3.1, however, the small temperature contrast in summer makes it very difficult to distinguish the Kuroshio from surrounding water in the August and September thermal images.)

Because of the way Ω is defined, it consists of a series of monotonically increasing ramps, each one terminated at a time when $\overline{\tau}$ drops below τ_c. Stage number is plotted with one unit change being equal to 3.7 Nm^{-2}day change in Ω. It is apparent that the loop-current stage is related to Ω: the open circles showing the stage number generally fall near the dotted line representing Ω.

Figure 6(a) shows the 1986–87 northeast-monsoon season. The first strong growth in Ω begins in late November, and by the middle of December Ω is over 7 Nm^{-2}day. Ω drops to zero in the beginning of January. The sea-surface temperature image on January 7 shows a well developed loop current as well as the Kuroshio extending a short distance on its direct path. The presence of this direct path is probably due to the drop in Ω. The next three clear images on January 16, February 11 and 17 all show a direct path and a loop current at the same temperature. This suggests at least part of the Kuroshio enters the loop current during the period between January 7 and February 17 (otherwise we would expect the loop current to appear cooler than the Kuroshio). A possible explanation is that after the winds drop in strength and then grow again at the beginning of January, the renewed winds transport water back into the path of the old loop current. Usually, after a pronounced drop in the wind causing Ω to drop to zero, a new loop current is formed when the winds regain their strength. For example, in January through March of 1989, the images show two instances of loop-current terminations following drops in Ω. In each instance, a new loop current forms when the wind's strength increases again (Fig. 6(c)). But perhaps in January–February, 1987 a new loop current is not formed because our criteria for loop-current termination are just barely fulfilled: no drop in Ω occurs in early January using $\tau_c = 0.077$ Nm^{-2} and $t_{ave} = 4$ days (Farris, 1995; Fig. 9). On February 8, Ω drops to zero and remains below 0.5 for the rest of the season. Accordingly the Kuroshio is on its straight path on March 20. A faint detached loop current is visible in this image. The loop is cooler, appears to be more circular and seems to have expanded slightly. The sea-surface temperature signal of this loop current is no longer visible on March 24.

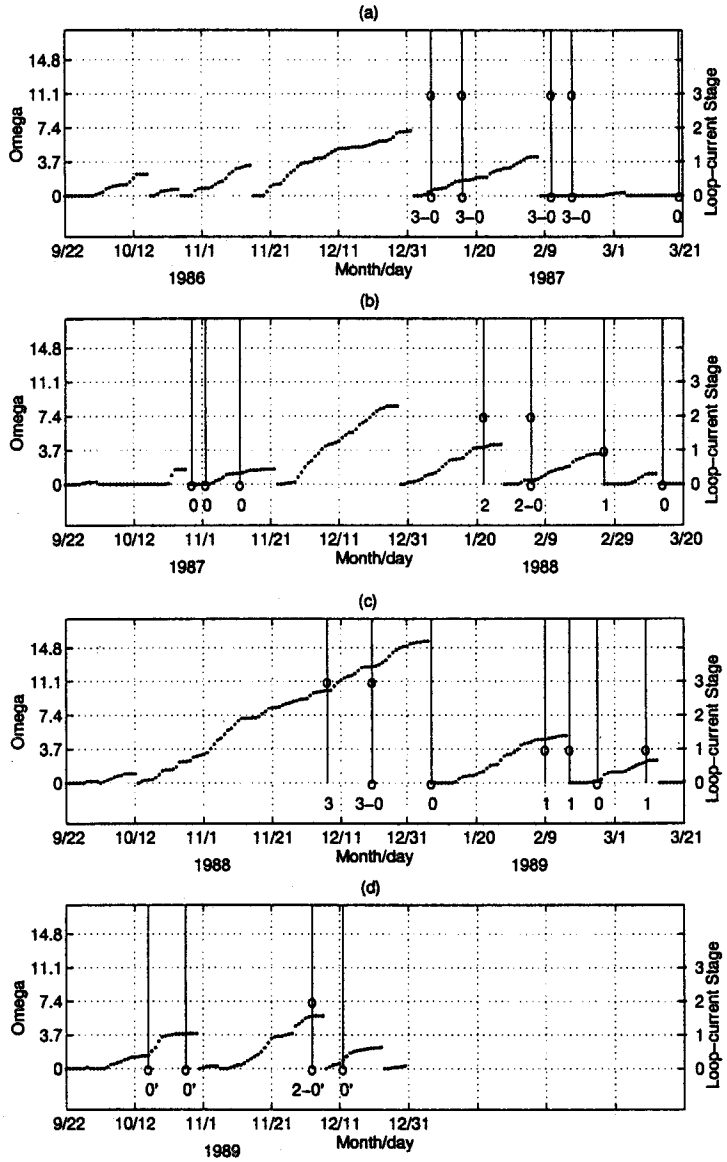

Fig. 6. Plot of integrated wind stress parameter $\Omega(t)$ in Nm^{-2}day, computed daily from Eq. (1) for the fall-winter sections of (a) 1986–87, (b) 1987–88, (c) 1988–89, and (d) fall of 1989. Time axis tick marks are at intervals of 20 days and are labeled month/day with the current year. Solid vertical lines indicate times at which the stage of the loop current could be determined from satellite thermal imagery. Numeric labeling of these lines indicates the loop-current stage determined from these satellite data. Loop-current stage is also indicated by elevation of open circle (or circles) on the vertical lines with a scale on the right-hand side of the plot. 3–0 indicates a branching of the Kuroshio at about 20°N with a Stage 3 loop to the west and a Stage 0 direct path to the east, 2–0 similarly indicates a combination of Stages 2 and 0 (in the 2–0 images the direct path extends only to 21° or 21.5°N). Primes on the labels for 1989 indicate that the mean path of the Kuroshio was shifted to the east (see 0′ panel in Fig. 3). Each panel starts on September 22 and ends on March 20 or 21, approximately a northeast-monsoon season. The southwest-monsoon seasons are not shown because during them there were no observed loop currents and Ω was always 0.

Figure 6(b) shows the 1987–88 northeast-monsoon season. All of December and most of January were cloudy, so our first clear loop-current image is on January 22, 1988. By this time Ω had risen to almost 4 Nm^{-2}day, and correspondingly the sea-surface temperature image shows the Kuroshio in a Stage 2 loop current. Ten days later, on February 1, Ω drops to 0, and the next image on February 5 shows both the Stage 2 loop current and the beginning of a Stage 0 direct path. After February 1, 1988 the winds regain their strength and Ω begins growing again. By late February Ω exceeds 3 Nm^{-2}day, and on February 26 we see a Stage 1 loop current. On February 25 Ω drops to near zero for the rest of the season, and on March 14 the Kuroshio is seen to be on its straight path.

Figure 6(c) shows the 1988–89 northeast-monsoon season. Beginning on October 13, Ω builds up continually until, in early January, it is nearly 15 Nm^{-2}day, the largest values reached in 1986–89. On December 7, with Ω already greater than 10 Nm^{-2}day, we see a fully-developed loop current. In the December 20 image both the loop-current path and straight path are visible. There is no corresponding drop in Ω; although the wind stress did drop below 0.078 Nm^{-2} for two days on December 19 and 20. In the next clear images on January 7 and 8 the Kuroshio is in its straight path and the loop current is very faint and quite separated from the Kuroshio. On January 7, Ω did drop to zero but it seems unlikely that the loop current could have cooled and drifted so much in one day. Perhaps a well-developed loop current is more susceptible to being cut off by direct flow than a less-developed loop current. In other words, perhaps τ_c increases (or t_{ave}

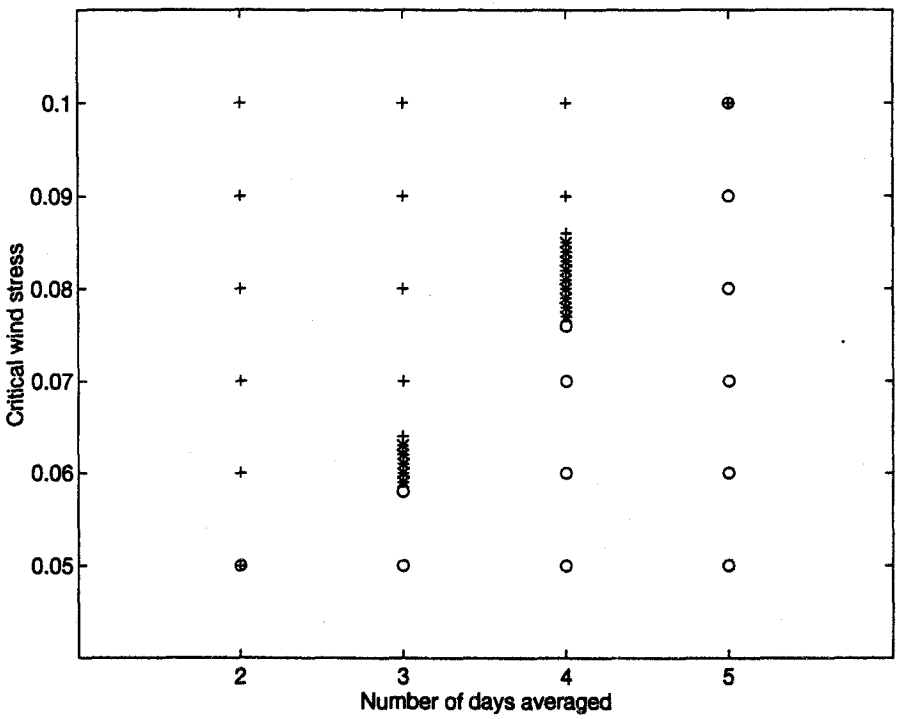

Fig. 7. Asterisks represent values of τ_c (Nm^{-2}) and t_{ave} (days) for which loop-current stage prediction error ε is a minimum (0.09). Circles represent values for which, in at least one instance, Ω continues growing when the images imply that it should drop. Plus signs represent values for which, in at least one instance, Ω drops when the images indicate that it should continue to grow.

decreases) when Ω—and hence the loop—becomes large. Throughout the rest of 1989 (Figs. 6(c) and (d)) loop-current formation and termination match Ω well.

We have calculated a parameter, ε, that quantifies how well Ω matches loop-current stage. In calculating ε we first used Ω, for a given τ_c and t_{ave}, to predict loop-current stage. We did this by multiplying Ω by a fraction called C and then rounding the result to the nearest integer. This integer was our predicted loop-current Stage, $\hat{S}$; since our observed loop-current stages stop at 3, if the integer was greater than 3 a value of 3 was substituted. This number was then subtracted from the loop-current Stage, S, seen in the corresponding satellite image, to get a difference for each satellite observation. The absolute values of these differences were summed and divided by the number of observations $n = 23$ to obtain the mean error:

$$\varepsilon = \frac{1}{n}\sum_{i=1}^{n}\left|S_i - \hat{S}_i\right|, \qquad \hat{S}_i = \min\left(3, \text{round}(C\Omega)\right),$$

where Ω is in $Nm^{-2}day$. When the observed loop-current stage is ambiguous (e.g., 3–0), the closer of the two values to $\hat{S}_i$ is assigned to S_i. This process was repeated with many values of C to find a minimum value of ε. The smaller ε is, the better the fit of Ω to the loop currents seen in the satellite images. We obtained a minimum value of ε for $\tau_c = 0.08$ Nm^{-2} and $t_{ave} = 4$ days; this minimum was $\varepsilon = 0.09$ with $C = 0.27 (= 1/3.7)$. This low value of ε results from correct predictions for all but two of the images, each of which is off by one loop-current stage.

We tested the robustness of these results in three ways. First we tested the sensitivity of the results to τ_c and t_{ave}. Figure 7 is a plot showing the effects of varying τ_c and t_{ave}. The asterisks represent values of τ_c and t_{ave} for which Ω agrees well with the images. For these values $\varepsilon = 0.09$. The circles represent values of τ_c and t_{ave} for which Ω continues to grow when at least one image shows loop-current development ceases. The plus signs represent values for which Ω drops to zero when at least one image implies it should continue to grow. Table 1 gives the minimum ε values and the corresponding C values for many points on Fig. 7. Not all low ε values represent good choices of τ_c and t_{ave}. Because of the way ambiguous loop-current stages are quantified, an observed 3–0 loop current, at a time when Ω had been less than $C/2$ (i.e., indicating Stage 0) since the beginning of the season, would contribute nothing to ε even though the Stage 3 part of the

Table 1. Minimum ε and corresponding C values for various combinations of τ_c (Nm^{-2}) and t_{ave} (days).

ε					C				
	t_{ave}					t_{ave}			
τ_c	2	3	4	5	τ_c	2	3	4	5
0.10	0.35	0.35	0.22	0.09	0.10	0.29	0.29	0.29	0.29
0.09	0.35	0.35	0.26	0.17	0.09	0.28	0.28	0.20	0.28
0.08	0.30	0.13	0.09	0.30	0.08	0.26	0.26	0.27	0.23
0.07	0.26	0.13	0.26	0.39	0.07	0.25	0.25	0.35	0.01
0.06	0.22	0.09	0.33	0.39	0.06	0.24	0.24	0.21	0.01
0.05	0.26	0.35	0.39	0.39	0.05	0.23	0.01	0.01	0.01

observation would then be inexplicable. An example is the $\varepsilon = 0.09$ value for $\tau_c = 0.10$ Nm^{-2}, $t_{ave} = 5$ days in Table l; for this reason, the corresponding point in Fig. 7 is not an asterisk.

The second way we tested the robustness of our results was to shift the wind data in time so that images from one year were compared to the wind data for the corresponding dates from a different year. With the winds shifted three different ways, the minimum ε was always 0.36 (Farris, 1995; Appendix C). Since ε is markedly less when the winds are matched correctly, these results support the validity of our relationship. Further support comes from the fact that the optimum C for the shifted wind data was always close to zero (≤ 0.05): because 17 of our 23 images are, at least in part, Stage $S = 0$, we would expect such a low C value for unrelated wind data.

Third, we tried using components of the wind stress at compass directions from 190° to 230° (direction of average northeast monsoon stress). But in each case the minimum ε was larger than the 0.09 value achieved with the 180° wind-stress component, as expected for Ekman transport through the meridional gap of the Luzon Strait.

5. Discussion

Our results support the hypothesis that the Kuroshio loop current in the South China Sea forms in response to the northeast monsoon. Under this hypothesis, we would expect the volume of water contained in the loop to be the sum of all the water driven in by the winds in excess of that which is entrained by the Kuroshio. This volume should be proportional to our parameter Ω. If we make the simplifying assumption that the excess Ekman mass transport

$$M_E = \frac{\tau - \tau_c}{f_o} L_B \tag{2}$$

through the strait of width L_B supplies the water contained in the loop, then the volume of this water would be

$$V = \frac{1}{\rho} \int M_E dt. \tag{3}$$

Here we note that for positive $\tau - \tau_c$, $\Omega = \int (\tau - \tau_c) dt$ so that $\int M_E dt = \Omega L_B / f_o$ and thus

$$V = \frac{L_B}{\rho f_o} \Omega. \tag{4}$$

Following Wang and Chern (1987b), we take $L_B = 2.4 \times 10^5$ m, and Coriolis parameter $f_o = 5.2 \times 10^{-5}$ s^{-1}. Then we use $\rho = 1030$ kgm^{-3} and $\Omega = 11.1$ Nm^{-2}day (for a well-developed loop current, $S = 3$). This gives $V = 4.3 \times 10^{12}$ m^3 which is within 20% of the 3.6×10^{12} m^3 volume estimated by Wang and Chern (1987b) from their measurements.

It seems reasonable that $t_{ave} = 3$–4 days. If one assumes the Kuroshio travels at about 0.7–1.0 ms^{-1}, it will cross the Luzon Strait (starting from 20°N, where it turns west when it forms a loop current) in this amount of time. Thus, after a loop current is formed, if the wind stress drops below τ_c for 3–4 days, the Kuroshio is able to complete its direct path across the Luzon Strait, "short-circuiting" the loop.

Although the northeast monsoon typically begins in September we did not observe loop current occurrences prior to November. We would expect such a delay because a typical wind stress $\tau = 0.15$ Nm^{-2} will, according to (1) take 50 days to produce a Stage 1 loop current ($\Omega = 3.7$ Nm^{-2}day).

6. Conclusions

Comparison of satellite observations with wind data supports the hypothesis that the northeast monsoon deflects the Kuroshio through the Luzon Strait to form the loop current. Indeed there appears to be a relationship between the loop-current stage and wind-stress history. This relationship is seen by calculating an integrated wind-stress parameter Ω. The larger Ω is, the more fully developed the loop current. When Ω goes to zero, the Kuroshio reverts to the direct path. A new loop current grows when the wind increases in strength again. The volume of water within the loop calculated from Ω is similar to a volume estimated from hydrographic data.

Acknowledgements

Kenneth Casey and Michael Alfultis kindly provided and pre-processed the sea-surface temperature and COADS data, respectively. The temperature data were obtained from the NASA Physical Oceanography Distributed Active Archive Center at the Jet Propulsion Laboratory, California Institute of Technology. Steven J. Worley at the National Center for Atmospheric Research provided Michael Alfultis with the COADS wind data.

This research was supported by the Office of Naval Research under grant number N00014-93-1-1046.

References

Adamec, D. and R. Elsberry (1985): Response of an intense oceanic current system to cross-stream cooling events. *J. Phys. Oceanogr.*, **15**, 273–287.

Cayula, J.-F. (1993): Automatic front detection using a sequence of sea surface temperature images. Ph.D. Thesis, University of Rhode Island, Narragansett, RI.

Chu, T.-Y. (1972): A study on the water exchange between Pacific Ocean and the South China Sea. *Acta Oceanographica Taiwanica*, **2**, 11–24.

Fan, K.-L. (1982): A study of water masses in Taiwan Strait. *Acta Oceanographica Taiwanica*, **13**, 140–153.

Fanning, A., R. Greatbatch, A. D. Silva and S. Levitus (1994): Model-calculated seasonal transport variations through the Florida straits: A comparison using different wind-stress climatologies. *J. Phys. Oceanogr.*, **24**, 30–45.

Farris, A. (1995): Effects of wind on the Kuroshio in the Luzon Strait. Master's Thesis, University of Rhode Island, Kingston, Rhode Island.

Guo, Z. and F. Wendong (1988): The Kuroshio in Luzon Strait and its transport during September 1985. *Tropic Oceanology*, **2**, 13–19.

Huang, Y. (1988): Temperature and salinity distributions in the South China Sea and adjacent waters. *Prog. Oceanogr.*, **21**, 493–501.

Nitani, H. (1972): Beginning of the Kuroshio. p. 129–163. In *Kuroshio*, University of Washington Press, Seattle, WA.

Shaw, P.-T. (1991): The seasonal variation of the intrusion of the Philippine Sea water into the South China Sea. *J. Geophys. Res.*, **96**, 821–827.

Shaw, P.-T. and S.-Y. Chao (1994): Surface circulation in the South China Sea. *Deep-Sea Res.*, **41**, 1663–1683.

Stramma, L., P. Cornillon, R. A. Weller, J. F. Price and M. G. Briscoe (1986): Large diurnal sea surface temperature variability: Satellite and in situ measurements. *J. Phys. Oceanogr.*, **16**, 827–837.

Su, J., B. Guan and J. Jiang (1990): The Kuroshio. Part I. Physical features. *Oceanography and Marine Biology Annual Review*, **28**, 11–71.

Uda, M. and T. Nakao (1973): Water masses and currents in the South China Sea and their seasonal changes. p. 161–188. In *The Kuroshio III*, Mongkol Karnpim Press and Publishing, Bangkok.

Vazquez, J., A. Tran, R. Sumagaysa, E. Smith and M. Hamilton (1995): NOAA/NASA Pathfinder AVHRR Oceans sea-surface temperature data set user's guide. Technical report, Jet Propulsion Laboratory, California Institute of Technology.

Wang, J. and C.-S. Chern (1987a): The warm-core eddy in the northern South China Sea, I. Preliminary observations on the warm-core eddy. *Acta Oceanographica Taiwanica*, **18**, 92–103.

Wang, J. and C.-S. Chern (1987b): The warm core eddy in the northern South China Sea, II. A simple mechanism for the establishment and development of the warm-core eddy. *Acta Oceanographica Taiwanica*, **18**, 104–113.

Wang, J. and C.-S. Chern (1988): On the Kuroshio branch in the Taiwan Strait during wintertime. *Prog. Oceanogr.*, **21**, 469–491.

Wu, J. (1982): Wind stress coefficients over sea surface from breeze to hurricane. *J. Geophys. Res.*, **87**, 9704–9706.

Xue, H., J. Bane and L. Goodman (1995): Modification of the Gulf Stream through strong air-sea interactions in winter: Observations and numerical simulations. *J. Phys. Oceanogr.*, **25**, 533–557.